Expectations from a Microlensing Search for Planets

S.J. Peale
Dept. of Physics
University of California
Santa Barbara, CA 93106
peale@io.ucsb.edu

ABSTRACT

The statistical distribution of the masses of planets about stars between the Sun and the center of the galaxy is constrained to within a factor of three by an intensive search for planets during microlensing events. Projected separations in terms of the lens Einstein ring radius yield a rough estimate of the distribution of planetary semimajor axes with planetary mass. The search consists of following ongoing stellar microlensing events involving sources in the center of the galaxy lensed by intervening stars with high time resolution, 1% photometry in two colors in an attempt to catch any short time scale planetary perturbations of the otherwise smooth light curve. It is assumed that 3000 events are followed over an 8 year period, but with half of the lenses, those that are members of binary systems, devoid of planets. The remaining 1500 lenses have solar-system-like distributions of 4 or 5 planets. The expectations from the microlensing search are extremely assumption dependent with 56, 138, and 81 planets being detected for three sets of assumptions involving how the planetary masses and separations vary with lens mass. The events can be covered from 54% to 62% of the time on average by high time resolution photometry from a system of three or four dedicated two meter telescopes distributed in longitude, so 38% to 46% of the detectable small mass planets (very short perturbations of the light curve) will be missed. But perturbations comparable to a day in length means all of the detectable Jupiters and Saturns will in fact be detected as well as a large fraction of the Uranuses. The ground based observational technique is robust, and meaningful statistics on planetary masses and separations can be inferred from such an intensive search, although these statistics, like the inferred data set, will also be dependent on the assumptions about the nature of the set of planetary systems. Finding most of many giant and sub giant planets outside the Einstein ring radii of their respective stars may be a better indicator of the frequency of Earth mass planets than direct detection of a few of the latter.

1. Introduction

The nearly circular and coplanar orbits of the planets around the Sun point to the formation of these planets from a highly dissipative disk of gas and dust. The inevitability of the natural formation of such a disk during the gravitational collapse of a rotating molecular cloud to form a star and the observational confirmation that essentially all recently formed stars possess such a disk (*e.g.* Strom *et al.* 1995) have led most to believe that planetary systems are a common result of the star formation process and therefore must be ubiquitous in the galaxy. The recent discovery of planetary sized bodies around several nearby stars (Mayor and Queloz, 1995; Marcy and Butler, 1996; Butler and Marcy, 1996; Gatewood, 1996) and about the pulsar PSR 1257+12 (Wolszczan and Frail, 1992) reinforces this confidence. However, except for the system around the M star Lalande 21185 (Gatewood, 1996), the inferred planets are in systems very much unlike our own, since planets comparable to or exceeding Jupiter's mass orbit very close to their primary stars. In fact, those companions in eccentric orbits about the ordinary stars are inferred to not be planets at all but were formed like binaries by fragmentation of a collapsing molecular cloud (Boss, 1996; Mazeh *et al.* 1996). This leaves massive planets comparable to or exceeding Jupiter's mass in nearly circular orbits about 51 Peg ($m \sin i \sim 0.45 m_J$, 4.2 day period), 55 Cnc ($m \sin i \sim 0.78 m_J$, 14.7 day period) and 47 UMa ($m \sin i \sim 2.4 m_J$, 1090 day period) contrary to our expectations of the stellar distances at which giant planets would be formed. (However, there is a mechanism by which such planets could migrate toward their stars after formation provided a nebula with significant mass persists sufficiently long (Lin, *et al.* 1996; Ward and Hourigan, 1989; Ward, 1996)). These discoveries imply that other planetary systems are likely to differ greatly from our own, with totally different distributions of planetary mass and character with distance from the star. In particular the number of terrestrial type planets in any system may be considerably different from expectations based on our own solar system.

The theory of the formation and evolution of planetary systems depends on only one example, whereas the recent discoveries of other planets indicate that a variety of scenarios leading to systems strikingly different from our own may be common. To understand the frequency of the particular chain of events that led to a planetary system like ours, where life was able to develop on one terrestrial planet, we need statistics not only on the occurrence of other planetary systems, but also on the planetary mass distributions as a function of the planet separation from the parent star. Giant planets close to their primaries may preclude the existence of terrestrial type planets in those particular systems. The recent discoveries of planets around other stars depended on detecting motion of the star relative to a system center of mass with the period of the planetary orbit. High precision Doppler spectroscopy and, in the case of Lalande 21185, high precision astrometry were used to determine the stellar motions. These techniques can provide information on planetary mass distributions and separations, where the Doppler technique is most sensitive to planets that are close to their stars and astrometry most sensitive to planets that are far away. Unfortunately, these observations are very demanding so relatively few stars can be monitored, and the observations must be continued for at least a planetary period for secure detection. Several decades of dedicated effort would be required to compile adequate statistics, and neither method is sensitive to terrestrial-mass planets at any separation.

The recently announced intention of the National Aeronautics and Space Administration to search for planets about other stars (Beichman, 1996) has as its goal the detection and characterization of terrestrial type planets orbiting stars within about 10 pc from the Sun. The instrumentation to be developed in this search depends on the distribution of planetary masses and in particular on the frequency of occurrence of Earth-mass planets. Planning this program requires the planetary statistics on a relatively short time scale, and it requires information on the frequency of occurrence of terrestrial-mass planets that is not obtainable by the radial velocity and astrometry techniques. Mao and Paczyński (1991) pointed out that a planet could be detected as a companion of a star by perturbing the light amplification curve of a more distant star (source) that is being gravitationally lensed (microlensing) by the nearer star (lens). Later Gould and Loeb (1992) derived a probability of nearly 20% for detecting a Jupiter about a solar mass star given that a microlensing event was taking place by assuming that a 5% perturbation of the light curve was detectable. Microlensing is a rare event, so millions of stars must be monitored in order to catch the few whose apparent brightnesses change in a system-

atic, achromatic way due to microlensing by a nearer star. The MACHO (MAssive Compact Halo Objects) collaboration has been remarkably successful in detecting approximately 100 microlensing events toward the galactic bulge over a two year period. The possibility of detecting at least 350 events per year with modest upgrades in technology together with a larger dedicated telescope at a good site (C. Stubbs, 1996, private communication) promises a means to gather planetary statistics at a reasonably rapid rate.

Although planets that orbit very close to their stars will not be detectable during a microlensing event, (The star and planet would act as a single lens.), the likely situation that most planetary systems will be dispersed more like our own motivates consideration of a dedicated microlensing search for planets. How many planets are likely to be detected in such a search, what is the nature of the data set, and what planetary statistics can be obtained? Here we construct examples of answers to these questions based on the Gould and Loeb (1992) probability of detecting a planet given that the planet's central star is acting as a lens during a microlensing event.

The source stars are treated as point sources in the derivation of this probability, which means that the application to small mass planets is not really valid. However, Bennett and Rhie (1996) have calculated detection probabilities given that a microlensing event is taking place for planet/(stellar lens) mass ratios $m/M = 10^{-5}$ and 10^{-4} at distances of 4 and 6.4 kpc and for sources at the galactic center of radii $3R_\odot$ and $13R_\odot$ as a function of the planet-star separation. These detection probabilities averaged over the mass function of the lenses for the $3R_\odot$ source radius and $m/M = 10^{-5}$ for a set of specific planetary orbital semimajor axes are remarkably close to the probabilities for the same fixed mass ratio from the point source calculation (Table 5). This indicates that our probabilities of detection for the Earth-mass planets for point sources may be representative to within a factor of 2. Even without this near agreement, our purpose here is to demonstrate the assumption dependence of the expectations from any microlensing search for planets, to show the effect of the stellar mass function where most of the lenses will be spectral class M stars, and to show how well a minimum data set can be interpreted. The variations in the number of planetary detections due to a variation in the assumptions is at least comparable to the errors in the estimates due to considering only the consequences for point sources.

We begin in Section 2 with a brief description of the simplest microlensing theory, and a description of the Gould and Loeb (1992) derivation of the probability of detecting a planet during a lensing event sufficient to allow one to understand the scaling of the published probability to arbitrary planet/star mass ratios and arbitrary mean lens distances. The distribution of events over a lens mass function like that of the stars in the local neighborhood is developed in Section 3, and it is used to average the scaled probability of detection of a planet of given mass, orbit semimajor axis, and average distance of the lens from the observer.

A sample observing program like that advocated in the Roadmap for the Exploration of Neighboring Planetary Systems (Tytler, 1995) is described in Section 4 after showing how the planet/star mass ratio and the planet-star separation normalized by the Einstein ring radius of the lens star is deduced from the microlensing light curve perturbed by the planet. Two color, high time resolution photometry of all ongoing microlensing events with 1% accuracy is advocated in this program. Two colors are necessary for redundancy, for distinguishing intrinsically varying stars, and to reduce uncertainties in some cases where the source star is resolved by the planet. The probability of being able to observe the high density star region in the galactic center (GC) from each of four specific observing sites at any specific time is used to develop the overall probability of observing the GC from at least one of the observatories as a function of the time of year. This is averaged over the time the GC is observable to show that this particular distribution of telescopes for a microlensing search could cover the ongoing events with high time resolution photometry about 54% to 62% of the time.

A reasonable data base of 3000 events assumed collected over an 8 year period is used in Section 5 to determine the number of planets that would be detected for three sets of assumptions about systems similar to the solar system. For one of these systems a sample planetary data set consisting of the planet/star mass ratios and planet-star separations is constructed from the appropriate probability distributions. An interpretation of this data set follows in Section 6 where it is assumed that only information from the detailed light curve is available with spectral classification of the brighter lenses used to further constrain these lens masses. Although only the planet/star mass ratios

follow from the light curves, the limited range of lens masses means a reasonable estimate of the distribution of planetary masses is obtained. Observational selection effects make the orbital semimajor axes of the planets less defined except for the general trend relative to the Einstein ring radius that reflects the assumptions about the nature of the systems.

In Section 7 we show how the finite sizes of the stellar sources affects the detection of Earth sized planets, where one gains because of the higher probability of the small planet affecting the light curve and longer duration of the event, but loses because of the much lower amplitude of the event. We also show examples of averaging the Bennett and Rhie (1996) detection probabilities (for finite sized sources) over the lens mass function, compare these probabilities to those obtained for point sources and point out the necessary steps for obtaining an overall probability of detecting small mass planets while accounting for the finite source sizes of the galactic bulge stars.

2. Microlensing and planet detection

The term microlensing comes from extra-galactic astronomy where the images of a quasar lensed by a single star in an intervening galaxy are separated by the order of microarcseconds (Chang and Refsdal, 1979). The images of a star in the galactic bulge that is lensed by an intervening star are separated by milliarcseconds, but the term is still applied. Fig. 1 shows the geometry of the gravitational lensing of a point source and the definition of several parameters. O, L and S refer to observer, lens and source respectively. The angle α is the general relativistic (small angle) deflection of a ray from the source that reaches the observer. The point source lens equation deduced from the figure is $r^2 - r_0 r - R_E^2 = 0$, where

$$R_E = \sqrt{\frac{4GMD_{OS}z(1-z)}{c^2}}, \qquad (1)$$

is the Einstein ring radius. The Einstein ring is the symmetric image of the source when it is directly behind the lens ($r_0 = 0$). Here G is the gravitational constant, M is the mass of the lens, c is the velocity of light and $z = D_{OL}/D_{OS}$. The circle centered on L in Fig. 1 is the Einstein ring on the lens plane. Solution of the lens equation $r_{1,2} = (r_0 \pm \sqrt{r_0^2 + 4R_E^2})/2$ yields the positions of the two images I_1 and I_2 outside and inside the Einstein ring respectively. The amplification (*e.g.*, Gould and Loeb, 1992),

$$A = \frac{u^2+2}{u\sqrt{u^2+4}}, \qquad (2)$$

is the factor by which the flux density from the source star is increased. It is found for each image as the transformation of areas from source to image coordinates with the results for both images being added together. Here $u = r_0/R_E$. The light curve of the event reaches a maximum when u has its minimum value of u_b. The time scale of the event is the time for the projected position of the source to move an Einstein ring diameter, $\tau = 2R_E/v \propto \sqrt{M}$ where v is the relative speed of the source projected onto the lens plane. The singularity in A at $u = 0$ is called the caustic point. This singularity is removed when the source is not a point source. Fig. 2 shows the light curves for a variety of impact parameters and illustrates the independence of the perceived time scale on the latter.

If the lens is a relatively close binary system, the lens equation relating coordinates of the images in the lens plane to the coordinates of the source in the source plane is now a vector equation (Schneider and Weiss, 1986). The quadratic lens equation for a single lens becomes two 5th order equations or a single fifth order equation in the complex plane (Witt, 1990). There are now either three or five images and the amplification is calculated for each image as before as the transformation of areas with the results summed for the total. The caustic point for the single lens is now one or two closed caustic curves in the source plane that transform into critical curves in the lens plane, where $A \to \infty$ when the point source is on a caustic. The singularity again vanishes for finite sized sources. There are three images when the source is outside a closed caustic curve and five when it is inside. A sharp peak in the light curve occurs when the source crosses a caustic with increased amplification while the source is inside. The simple, bell shaped light curve for a single lens can become quite complicated for a binary lens but also quite informative (*e.g.* Alard, *et al.* 1995).

When the second member of the binary system is a planet, the small mass of the planet compared to the star leads to a significant deviation of the light curve from that of the star without the planet only if the one of the two unperturbed images of the source comes close to the planet's projected position in the lens plane (Gould and Loeb, 1992). Fig. 3 shows an

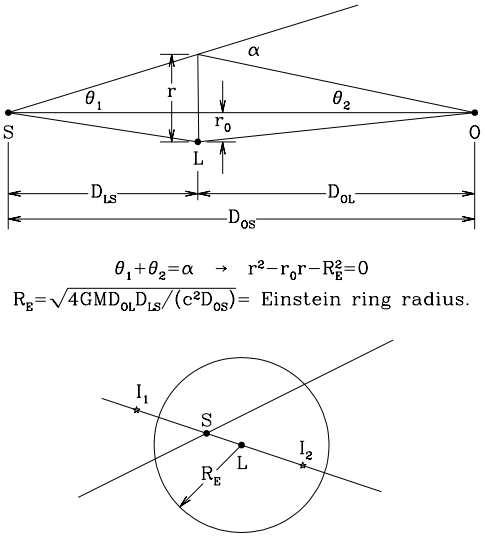

Fig. 1.— Geometry of a microlensing event and definition of parameters. The circle in the lower diagram is the Einstein ring of the lensing star and I_1, and I_2 are the images of the source S. O, L and S refer to Observer, Lens and Source respectively.

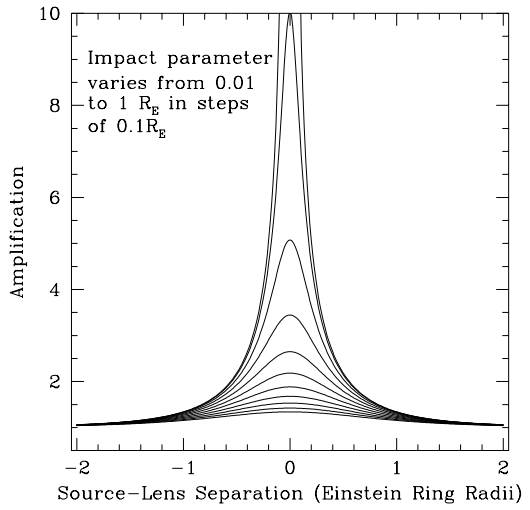

Fig. 2.— Microlensing light curves for several impact parameters of the relative motion of source and lens stars. The independence of the time scale of the event on the impact parameter is illustrated.

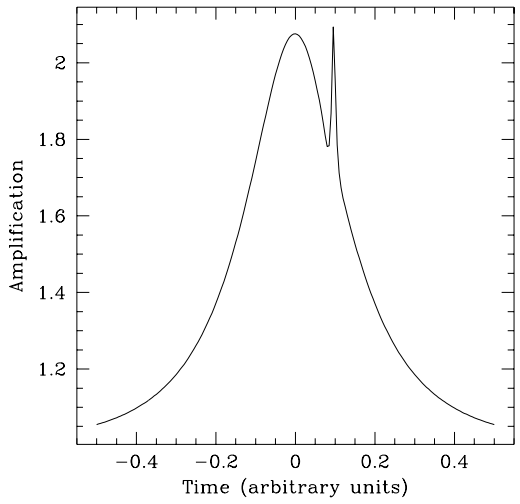

Fig. 3.— Example of a microlensing light curve perturbed by a planet. The planet/star mass ratio $m/M = 0.001$ and the planet is located $1.3R_E$ from the lens. (After Gould and Loeb, 1992)

example of such a perturbed light curve, where the planetary signature is larger than the simple sum of the gravitational lensing of the star plus the planet because the planet is focusing light already focused by the central star. For an event involving a lens with a planetary companion, the planet can affect the light curve of a point source by at most a very short fraction of the total time of the event as shown in Fig. 3, and for most events, the planet will not reveal its presence. However, for a point source near the galactic center being lensed by a solar mass star at 4 kpc from the Sun, the probability that a Jupiter mass planet 5.2 AU from the star will cause at least a 5% deviation from the unperturbed light curve some time during the event is about 0.17 (Gould and Loeb, 1992). (An event is said to occur when the lens and source come within an Einstein ring radius of the lens of each other.) This high probability results from the semimajor axis being near the Einstein ring radius of the star where the probability is maximized, but there is a considerable range of semimajor axes ($2.4\,AU \leq a \leq 7.3\,$AU for this case) where the probability exceeds 0.1 (Gould and Loeb, 1992). David Tytler (private communication, 1995) has coined the term "lensing zone" for this range of semimajor axes

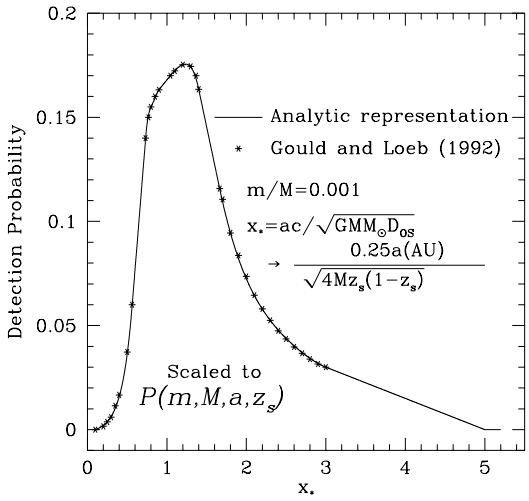

Fig. 4.— Analytic representation of the probability of detecting a planet with $m/M = 0.001$ given that an event is taking place, where a point source is assumed and where a 5% perturbation of the light curve anytime during the event is assumed detectable. The curve has been linearly extended beyond the Gould and Loeb data. The second form of x_* is to account for the scaling of the position of the lensing zone for various average fractional distances of the lens z_s and lens masses M. (M is normalized by $M_\odot$.)

where the probability of detection is high.

An analytic representation of the Gould and Loeb (1992, Fig. 8) detection probability for a planet/star mass ratio $m/M = 0.001$ and for a 5% detection threshold (Appendix A) is shown in Fig. 4, where $x_* = ac/\sqrt{GMD_{OS}}$ is the scaled semimajor axis, and where the curve has been linearly extended for $(3 \leq x_* \leq 5)$. We shall use this probability of detection in generating a sample data set for a microlensing planet detection program, but several qualifications and extensions are necessary. First the curve was derived under the assumption that the sources are point sources. The probabilities of detection are thus representative only as long as the angular size of the Einstein ring of the planet is large compared with the size of the source. This follows because a point source must be inside the Einstein ring of a lens for significant amplification and therefore only a fraction of a finite source can be amplified by a small lens with a consequently smaller perturbation of the light curve. At the same time, there is a larger probability that some part of the now finite sized image of the source will encounter the planet in the lens plane. Recent calculations by Bennett and Rhie (1996) have demonstrated that this enhanced probability of planet encounter may more than compensate for the lower amplitude of the perturbation in the sense that their maximum probability of detection is about twice the maximum probability of detection for a point source with a planet/star mass ratio of 10^{-5}. Averaging the Bennett and Rhie detection probabilities over the lens mass function in Section 7 yields probabilities of detection close to those obtained with a point source, so small mass planet detections determined with the point source assumption should be within a factor of 2 of those accounting for the finite source size.

Next, the Gould and Loeb probability was derived by averaging over a distribution of lenses along a particular line of sight that was displaced about 4° from the direction to the galactic center yielding a uniform distribution of lenses. Other lines of sight for the assumed spatial distribution of stars in the galaxy would yield different probabilities, but not significantly so. The fact that the number of detected events toward the galactic center was about three times that expected from the distribution of stars assumed in the Gould and Loeb analysis (Alcock, *et al.* 1995) will affect the probabilities of detection by moving the position of the average lens closer to the center of the galaxy thereby reducing the size of the Einstein ring radii (Eq. (1)). This follows since the excess lenses are thought to be located in a bar-like distortion of the galactic bulge distribution of stars oriented towards the Sun (Zhao *et al.* 1995). An approximate correction for this effect is made below.

The correction in the probability for moving the average lens closer to the source as well as scaling the probability for different values of m/M will be better understood if we outline how the probability of detection is determined. If $m/M \to 0$, the binary lens solutions go to the single lens case with the two unperturbed images described above. For small m/M only one of the images will be significantly affected when the planet approaches a separation from the unperturbed image position comparable to planet's own Einstein ring radius, and the new images will be close to the unperturbed position of the image. The amplification is calculated as before as the sum of the amplifications of each image. As the planet must be

close to the unperturbed image position for significant perturbation of the light curve, contours of planetary positions for a given percentage perturbation of the light curve will be grouped close to the unperturbed image position with the percentage perturbation decreasing for contours further away from that position.

In Fig. 1 we can imagine a contour of the planetary position in the lens plane corresponding to a 5% perturbation surrounding each of the two nonperturbed image positions. Examples of these contours are shown in Fig. 2 of Gould and Loeb (1992). If the planet is inside one of these contours drawn in the lens plane, the perturbation of the light curve will exceed 5%. As the source and lens pass, the unperturbed images describe arcs in the lens plane (see Fig. 1), and the loci of the contours as the images change their positions define two areas in the lens plane. If the projected position of the planet is inside either of these areas, there will be a perturbation of the light curve exceeding 5% sometime during the event and the planet will be detectable. The probability of the planet detection sometime during the event is just the probability that the planet is within either of the two areas. Finally the probability is determined for and averaged over all impact parameters less than the Einstein ring radius.

The first step in determining this probability is to assume that a planet with semimajor axis a has a uniform probability distribution over a sphere of radius a to account for random orbit inclination and phase. Then the probability that the planet has a projected separation between r and $r + dr$ is

$$p(r)dr = \frac{rdr}{a^2\sqrt{1 - r^2/a^2}}, \tag{3}$$

and the probability that the planet is between r and a is $F(r) = \sqrt{1 - r^2/a^2}$. If we normalize the distances by the Einstein ring radius R_E from Eq. (1),

$$F(x_p, z) = \left[1 - 4z(1 - z)\frac{x_p^2}{x_*^2}\right]^{1/2} \tag{4}$$

represents the probability that the planet will be located between $x_p = r/R_E$ and a/R_E from a lens located at fractional distance z to the source with $x_* = ac/\sqrt{GMD_{OS}}$ as before. Gould and Loeb (1992) average Eq. (4) over the line of sight weighted by the probability that an event will occur to obtain

$$F(x_p) = \frac{\int_0^{1/2-z_0} \cdots dz + \int_{1/2+z_0}^1 R_E(z)\nu(z)F(x_p, z)dz}{\int_0^1 R_E(z)\nu(z)dz}, \tag{5}$$

where $\nu(z)$ is the spatial density distribution and where $z_0 = 0$ if $x_p < x_*$ and $z_0 = 0.5\sqrt{1 - x_*^2/x_p^2}$ if $x_p > x_*$. Although this is the form used by Gould and Loeb in their calculations, it differs from their Eq. (3.8) in that the integral is separated into two segments. The split limits are necessary since the integrand becomes undefined when $x_p > x_*$. At $z = 1/2$, $x_p > x_*$ implies $r > a$ which is clearly impossible. As z moves away from 1/2, $x_p = r/R_E$ gets larger as R_E gets smaller. So to have a value of r still inside the maximum planetary separation from the star for larger x_p, the integration can extend only over those values of z where large x_p still corresponds to $r < a$.

The particular form of $\nu(z)$ chosen by Gould and Loeb places the average lens near 4 kpc from the Sun. If we let $\nu(z) = C\delta(z - z_s)$ where C is some constant, all of the lenses are at $z = z_s$ and $F(x_p) = F(x_p, z_s) = \sqrt{1 - 4z_s(1 - z_s)(x_p/x_*)^2}$. The probability distribution

$$-\frac{dF(x_p)}{dx_p} = \frac{4x_p z_s(1 - z_s)}{x_*^2\sqrt{1 - 4z_s(1 - z_s)(x_p/x_*)^2}}$$

is strongly peaked at a removable singularity at $x_* = x_p\sqrt{4z_s(1 - z_s)}$. This is where the probability of finding the planet per unit area in the lens plane would be maximal. Now the contours surrounding the unperturbed image positions within which the perturbation to the light curve exceeds 5% are maximal in size when the image comes close the the Einstein ring and the locus of contour areas during the event is likewise maximized. As the planet must be near the image to be inside the contours, $x_p \sim 1$ (*i.e.* planet near the Einstein ring). The combination of the largest areas in the lens plane for which the perturbation of the light curve would exceed 5% sometime during the event, if the planet were inside the area, with the maximum probability per unit area corresponds to the highest probabilities for finding the planet. So for x_p near 1, $x_* \sim \sqrt{4z_s(1 - z_s)}$ corresponds to the peak in the probability curve. For $z_s = 1/2$ the peak should be near $x_* = 1$, and we see from Fig. 4 that placing all the lenses at $z = 1/2$ gives a peak in the probability of detection near the peak that was obtained for the average lens being at $z = 1/2$. So for the average

lens being at a value of z other than 1/2, we shift the lensing zone by $\sqrt{4z(1-z)}$. This is equivalent to writing $x_* = 0.25a/\sqrt{4Mz_s(1-z_s)}$ in reading the probabilities from Fig. 4, where a is in AU, M is in units of $M_\odot$, z_s here is approximately the value of z for the average lens, and other constants have been evaluated.

Next we must scale the probability of detection to planet/star mass ratios m/M other than the value of 0.001 appropriate to Fig. 4. We note that the size of the 5% contour around the unperturbed image position in the lens plane scales as $\sqrt{m/M}$ (Gould and Loeb, 1992). As the arc described by unperturbed images is long compared to any dimension across the contours and this arc is independent of m/M, only the dimension of the area of the locus of contours perpendicular to the image arc is affected by a change in m/M, so the area of the locus of 5% contours for the complete event scales as $\sqrt{m/M}$. Since the probability per unit area of the planet falling into the area of the locus of contours does not vary much over the area, the probability is changed approximately as the area is changed. Hence, for a given value of x_*, we need but multiply the probability by $\sqrt{m/0.001M}$ to obtain the probability of detection for an arbitrary planet/star mass ratio. We will thus represent the Gould and Loeb probability curve in Fig. 4 so scaled and shifted as $P(a, m, M, z_s)$. This is the probability, during a lensing event, of detecting a planet of mass m, with semimajor axis a, orbiting a lens star of mass M located at a mean fractional distance z_s. Below we will average this probability over the mass function for particular sets of values of a, m, z_s, but first the distribution of events over the mass function must be developed.

3. Distribution of the events over the lens mass function

We shall assume that the mass function for local stars is representative of the stars between us and the center of the galaxy. This assumption will probably be most in error for masses larger than about $1.5M_\odot$, since more massive lenses within the galactic bulge will have evolved off the main sequence and thereby will have lost mass on their way to becoming white dwarfs or neutron stars. The mass function used here is an analytic approximation derived from the multiplicity corrected present day mass function for main sequence stars given in Table 1 and Fig. 5 of Basu and Rana (1992). We consider only the range of masses $0.08 \le M \le 2.0$ because of the very small fraction of stars of higher mass and because of the completed evolution of the older possible lens stars in the near side of the galactic bulge. M is expressed in units of the solar mass $M_\odot$. This mass function of main sequence stars neglects the contribution of white dwarfs and neutron stars to the lens population, but these latter stars are expected to be a small fraction of those stars remaining on the lower main sequence. The mass function is represented by (based on Basu and Rena, 1992)

$$\begin{aligned} \phi(M) &= 48.39M^{-1} && 0.08 \le M \le 0.5327, \\ &= 13.73M^{-3} && 0.5327 \le M \le 1.205, \\ &= 28.04M^{-6.83} && 1.205 \le M \le 2.0, \end{aligned} \quad (6)$$

where $\phi(M)dM$ is the number of stars/pc^2 in the solar neighborhood in the mass range dM about M integrated perpendicular to the galactic plane.

The fraction of stars in the range dM about M is found by dividing $\phi(M)dM$ by the integral of $\phi(M)dM$ over $0.08 \le M \le 2.0$, but this is not the fraction of microlensing events to be expected for lenses in mass increment dM. This follows from our definition of an "event" as the lens and source coming within an angular radius of each other equal to the Einstein ring angular radius R_E/D_{OL} of the lens. The dependence of R_E on M (Eq. (1)) means that a more massive lens has a greater probability of having a source pass within its Einstein ring radius than a less massive lens.

To evaluate the distribution of events over the mass function, we assume first for simplicity that $D_{OS} = 8\,\mathrm{kpc}$ is the same for all the source stars in the galactic bulge, so that $z = D_{OL}/D_{OS}$ is the fractional distance of the lens to the center of the galaxy. If $v_\perp(z)$ is the magnitude of the component of velocity of a single lens perpendicular to the line of sight, and N is the number of sources per unit solid angle toward the galactic bulge, $Nv_\perp(z)2R_E(M,z)/(z^2D_{OS}^2)$ is the number of encounters (events) per unit time experienced by the single lens of mass M at fractional distance z. Next, let $\nu(r)$ be the number density of stars at distance r, such that $\nu(r)dr$ is the areal density of stars for the range between r and $r+dr$. Let $f(M)dM$ be the fraction of stellar masses between masses M and $M + dM$, which is constructed from $\phi(M)$ (Eq. (6)) as described above. Setting $r = D_{OS}z$, we have $f(M)dM\nu(z)D_{OS}^3z^2dz$ is the number of stars between

M and $M + dM$ per unit solid angle that are in the slab between z and $z + dz$. Multiplying this by the events per unit time due to a single lens of mass M at z and inserting the explicit M and z dependence into R_E yields

$$2\sqrt{\frac{4GM}{c^2}}D_{OS}Nf(M)dM\int_0^1 \nu(z)\langle v_\perp(z)\rangle\sqrt{z(1-z)}dz \tag{7}$$

as the number of events per unit solid angle per unit time due to lenses between M and $M + dM$ over the entire line of sight. Here $\langle v_\perp \rangle$ is an average transverse speed. Then from Eq.(7),

$$\mathcal{F}(M)dM = \frac{\sqrt{M}f(M)dM}{\int_{0.08}^{2.0}\sqrt{M}f(M)dM} \tag{8}$$

represents the fraction of events due to lenses with masses between M and $M + dM$, where common factors from Eq. (8) have been cancelled in numerator and denominator. The probability of detection of a planet of mass m, semimajor axis a, located at average fractional distance z_s weighted by the distribution of events over the mass function along the line of sight is

$$P(m, a, z_s) = \int_{0.08}^{2} \mathcal{F}(M)P(m, M, a, z_s)dM. \tag{9}$$

The distribution of this probability over the m, a plane is shown in Fig. 7 for the case where the planetary mass m and semimajor axis a are invariant over the lens mass function. It is used in section 5 to deduce sample results from a dedicated microlensing search for planets, but first in the following section we define a representative observing program that accounts for observing constraints.

4. Sample Observing Program

Recall that the planet-image separation must be on the order of the Einstein ring radius of the planet or less to cause a significant perturbation of the single lens light curve. The time scale for the whole event is the time required by the source to traverse an Einstein ring diameter of the star (see Fig. 2). The time scale of the planetary perturbation is the time required for the image to traverse the Einstein ring diameter of the planet, which is comparable to the time required for the source to traverse the Einstein ring diameter of the planet. The relative transverse speed of the source is the same for both cases, so the ratio of the time scale of the planet perturbation to the time scale of the event is just $\sqrt{m/M}$ (see Eq. 1). If an event perturbed by a planet with mass ratio 0.001 is observed to last 45 days, the planet perturbation would last only about 1.4 days. For a point source, a perturbation by an Earth mass planet about a solar type star ($m/M = 3 \times 10^{-6}$) would last only about 1.8 hours for the same 45 day main event. However, the effect of the finite size of the source on the detection of small mass planets is profound, where a perturbation of the light curve is both reduced in amplitude and extended in duration beyond the 2 hours expected for a point source. For this reason, the observing strategy must be fundamentally different for detecting the small mass planets. We will discuss this in more detail in Section 7. If a 5% perturbation of a light curve is considered detectable, all events would have to be photometrically monitored with about 1% accuracy at time intervals no longer than about one hour to detect a perturbation by Earth-mass planets and if a perturbation is detected, at intervals of a few minutes thereafter on that particular light curve for the duration of the perturbation. In reality, the time scale for the planetary perturbation for a given mass ratio will vary somewhat depending on the angle that the source crosses the given magnification contours in the source plane. But that angle is known from the position of the planetary perturbation on the unperturbed light curve. This defines the intersection of the source trajectory with the line connecting the lens and planet. From this angle and an accurate, high time resolution light curve obtained during the perturbation, one can model the light curve and refine the determination of the mass ratio.

The ratio of the planet-star separation and the Einstein ring radius r_p/R_E also follows from the position of the planetary perturbation on the unperturbed light curve. If the perturbation is removed, the unperturbed amplification yields $u = r/R_E$ from Eq. (2). For each value of u, the positions of the two unperturbed images are known and the planet must be near one or the other image to have perturbed the light curve. The selection of the correct image between the two can follow from the modeling of the light curve. If the caustic in the source plane is intercepted by the point source, the planetary position is known to within the Einstein ring radius of the planet.

David Tytler (1995) has suggested a telescope distribution and observing program to accomplish

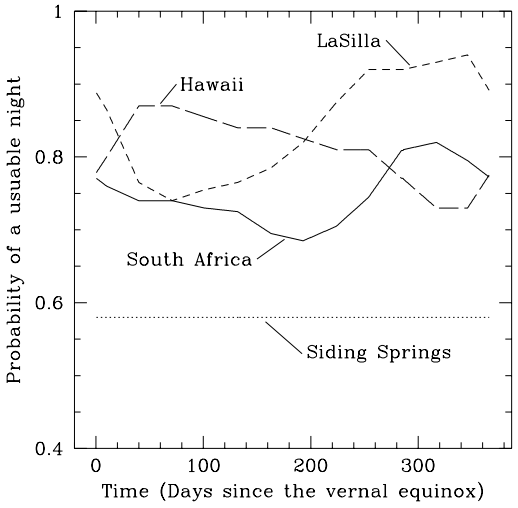

Fig. 5.— Probability of a usable night as a function of the time of year for four observatories that are suitable locations for dedicated telescopes in a microlensing search for planets.

the necessary observations. One of four two meter telescopes at established sites distributed as widely as possible in longitude in the southern hemisphere would monitor several tens of millions of stars in the galactic center (GC) in two colors at least once a night whenever the bulge is observable. This "survey telescope" would discover as many microlensing events as possible using a technique that is currently being used successfully by the MACHO collaboration (Alcock *et al.* 1995, 1996). The three "followup telescopes" would photometrically monitor each of the ongoing microlensing events in two colors at the high accuracy and high time resolution described above. We have arbitrarily added a fourth followup telescope in Hawaii.

The locations of three developed observatory sites in the southern hemisphere separated maximally in longitude plus Hawaii in the northern hemisphere are shown in Table 1. Weather, equipment problems and maintenance prevent 100% coverage of the events with high precision, high time resolution photometry. The fraction of usable nights (spectroscopic) at each observatory site is shown in Fig. 5 where the curves are constructed from monthly averages for LaSilla (http://lwh1.ls.eso.org) and South Africa (J. Caldwell, Private communication, 1996), quarterly averages from Hawaii (J. Glaspey, Private communication, 1996), and yearly averages from Siding Springs where summer and winter are comparable (J. Mould, Private communication, 1996). The GC can only be observed from a given site at some time t when it has a zenith angle less than 70° while the solar zenith angle is greater than 105°. If these criteria are satisfied, the probability that the GC is observable at the particular time is taken from Fig. 5. Otherwise the probability of observing the galactic center from that site at that time is zero.

The probability that the GC is observable from at least one of the observatories at any instant is then just the union (*e.g.* Feller, 1957, p. 88) of the probabilities for each site at that instant. This union of probabilities differs from that for one or another of the sites only when the GC is simultaneously observable from more than one site. The sum $\sum_{i=1}^{n} P(t_i)\Delta t_i$ gives the fraction of a day that the GC can be observed, where $P(t_i)$ is the probability of observation at time t_i and $\Delta t_i = 1/n$ is an increment of a day with n being large but otherwise arbitrary. The probability of being able to observe the galactic center on a given day so calculated and thus to make photometric measurements of lensed stars is shown in Fig. 6 as a function of time. The maximum observability occurs in the southern winter and drops to zero when the Sun is near the position of the galactic center during southern summer. There would be a period of time spanning day 90 in Fig. 6 where the probability of observing the GC would be unity if the weather were always perfect and equipment always worked, since the GC would always be observable from at least one of the sites throughout the day. The addition of Hawaii to the three southern sites gives a significant increase in the probability of observation because of its low northern latitude and because of its ideal location in longitude between Siding Springs and LaSilla.

As the Sun approaches the position of the galactic bulge in the sky, the duration of dark sky while the GC is up shrinks to the point where all of the ongoing events cannot be covered with high precision photometry in the time available. In fact there is a point beyond which the survey telescope cannot cover all of the fields in its program, and observations would probably cease for a time longer than the 71 days when the GC is completely blocked by the Sun in Fig. 6. The MACHO group requires about an hour to cover 24 fields toward the galactic bulge with an

Observatory	Latitude (deg.)	E. Longitude (deg.)
LaSilla	-29.25	289.27
Siding Springs	-31.27	149.06
South Africa	-32.38	20.80
Hawaii	+19.83	204.52

Table 1: Location of selected observatory sites.

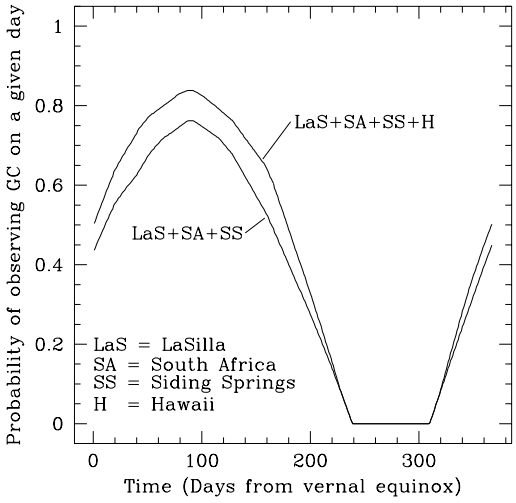

Fig. 6.— Probability of observing the galactic center (GC) on a given day. A probability of 1 would indicate that the GC was observable at all times during the day from one or more observatories. The GC is considered observable if the zenith angle of the GC is less than 70°, the zenith angle of the Sun is more than 105° and the night is usable.

additional hour of overhead (Alcock, *et al.* 1966; C. Alcock, private communication, 1996). If we assume that two hours is the minumum amount of dark time for observing the GC, the 71 day exclusion region in Fig. 6 is expanded to about 120 days, leaving 245 days as the maximum span of time per year for observing the GC in a microlensing survey and for followup photometry. If we center the 245 day span over the peak probability in Fig. 6 and average the probability over this span of time, we obtain the average fraction of the time when the galactic center can be monitored with high time resolution photometry during observed microlensing events. This fraction of 0.54 for just the three southern observatories is increased to 0.62 with the addition of a fourth telescope in Hawaii.

The approximately 58% average coverage for the assumed configuration of telescopes means that a little less than half of the planetary perturbations of microlensing light curves *of very short duration* will be missed. However, if the duration of the perturbation to the light curve exceeds a day, as it would in most cases for a Jupiter mass planet, the curves in Fig. 6 represent the fraction of the perturbation that could be monitored on the average where the probability of detecting the perturbation is essentially unity. This latter assertion follows since the probability of *all* of the sites having unusable nights on a given day is

$$P_{\rm all\,cloudy} = \prod_i (1 - P_i) \approx 3 \times 10^{-3}\,{\rm to}\,3 \times 10^{-4},$$

where P_i is the probability of a usable night at the ith observatory taken from Fig. 5, and where the range of values results from the variation in the weather conditions during the year. The fraction of the longer perturbations of the light curve that must be followed for meaningful interpretation is not large if the groups of high precision points are well distributed as they normally would be as the event is passed from one observatory to the next.

A few more of the small planets will be missed because of abandoning complete coverage to take measurements of ongoing perturbations every few minutes, but these will be neglected in the following. The probability of observing the GC in Fig. 6 would approach unity for a time spanning the southern winter if an arbitrary number of followup telescopes could be distributed more or less uniformly in longitude near $-30°$ latitude (*e.g.*, see Gould and Loeb, 1992). The impracticality of developing many new sites and necessary ocean gaps preclude this ideal.

Alcock *et. al.* (1996) found 43 likely microlensing events in the first year galactic bulge data where

12.6 million stars were monitored for 190 days. For the same detection efficiency, following a little more than 100 million stars would allow the detection of 350 events per year. However, from the Alcock *et al.* data, the optical depth for microlensing events for the distance from the Sun to the center of the galaxy is $3.9^{+1.8}_{-1.2} \times 10^{-6}$, which is based on the 13 lensed giants that are concentrated near the galactic center. An overall optical depth, based on the entire data set, was estimated to be $2.43^{+0.54}_{-0.45} \times 10^{-6}$, where the latter number is thought to be smaller because some of the main sequence sources were closer to us than the center of the galaxy. Both optical depths account for empirical determinations of the detection efficiency, which never exceeded 0.4 and decreased toward zero as event time scales approached a few days. These optical depths imply that far fewer than 100 million stars would have to be monitored to detect 350 events per year if the detection efficiency were increased by using a larger telescope at a better site along with only modest improvements in technology and observational procedures (C. Stubbs, private communication, 1996). If each event lasts an average of about 40 days (Alcock, *et al*, 1996), 350 events in a 190 day observing period would mean that almost 75 stars would be lensed at any one time. With continued improvements in technology and observing procedures, the observation of about 3000 microlensing events over about an 8 year period is not an unreasonable goal. These events would be covered with precise, high time resolution photometry about 58% of the time on average. We will adopt these numbers in the examples to follow, where the number of detected *small* planets scales directly both with the total number of events and with the percentage of photometric coverage and the number of large planets with just the total number of events.

5. Sample expectations from a microlensing search

What is expected from any microlensing search for planets depends entirely on what is assumed about the nature of likely planetary systems. It is guaranteed that the distribution of planet properties we find is going to be unexpected, but to illustrate some examples, and to show the assumption dependence of the expectations, we shall base our model systems on our own solar system. In about half of the 3000 assumed events, the lens will be a member of a binary system although this binary nature will usually not be revealed. (Close binaries will act as a single lens and binaries separated by more than twice the Einstein ring radius of the more massive member will [usually] act as two separate lenses. Attempts to obtain a secure distribution of binary separations are frustrated by severe observational bias (D. Popper, private communication, 1996).) To be conservative, we assume that none of the binary systems have any planets, but to be equally optimistic we assume that all of the remaining 1500 events involve lenses with planetary systems similar to our own, but with only four or five planets.

All 1500 remaining lenses have a Venus ($m/M_\odot = 2.5 \times 10^{-6}$) at 0.7 AU, and an Earth ($m/M_\odot = 3 \times 10^{-6}$) at 1 AU, but only half or 750 lenses have a Jupiter ($m/M_\odot = 1 \times 10^{-3}$) at 5 AU and a Saturn ($m/M_\odot = 3 \times 10^{-4}$) at 10 AU. The other 750 lenses have Uranuses ($m/M_\odot = 5 \times 10^{-5}$) at the distances of the Jupiters and Saturns and, for these latter systems, an extra Earth at 2.5 AU. It is difficult to make a Jupiter in the current planet formation paradigm within the observationally estimated lifetimes of preplanetary disks, so we remove Jupiter from half of the systems. The extra Earth at 2.5 AU is motivated by Wetherill's (1994) calculations showing the persistence of Earth mass planets in the asteroid belt if Jupiter is absent. Given these systems around 1500 of the lenses, how many of the planets would be detected in the dedicated microlensing search described above? What is the nature of the minimum data set that would be obtained, and how well could it be interpreted? Before attempting to answer these questions, we must make assumptions concerning the variation of the system properties with the mass of the central star.

We shall determine the expected number of detected planets for three distinct sets of assumptions: 1. The planet-star mass ratios and separations remain invariant for all stellar masses M. This means that smaller stars have smaller planets, but that the Earths, for example, will always be at 1 (or 2.5) AU regardless of the value of M. There is some weak justification for assuming that the planet-star separations are the same regardless of the mass of the primary, at least for Jupiters, since the ice condensation point in a preplanetary nebula where Jupiters are thought to form may always be near 5 AU (Boss, 1996). 2. The planet-star mass ratios remain invariant, but the separations are always the same fraction of the Einstein ring radius at $z = 0.5$. Here smaller

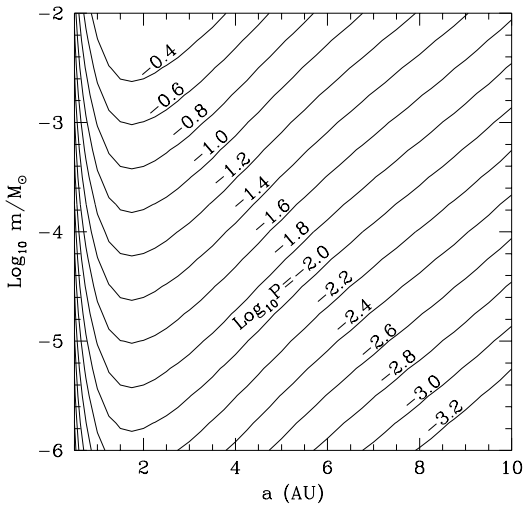

Fig. 7.— Distribution over the m, a plane of the probability of detecting a planet $P(m, a, z_s)$ during an ongoing microlensing event for the case where the average fractional distance to the lens $z_s = 0.8$ and where the planetary mass m and semimajor axis a are assumed invariant over the lens mass distribution.

stars have smaller planets, but the planets move closer to their central stars as M decreases. 3. The masses and separations remain invariant instead of the mass ratios and separations. In this last case, the Jupiters for example will always have $m = 0.001 M_\odot$ for all values of M and will always be 5 AU from their central stars.

The results of applying Eq. (9) for the three sets of assumptions and two values of z_s are given in Table 2, and Fig. 7 shows the probability distribution over the m, a plane for the model corresponding to the last column. In this application of Eq. (9), each planet type is treated independently, so the probabilities include the perhaps unlikely situation of detecting two planets around the same star. Multiplying the number of assumed planets by these probabilities yields the number of each of the planets that are detectable. We shall assume that the fraction of the detectable small planets (Earths and Venuses) that are actually characterized is the same as the 58% averaged maximum coverage, but that all of the detectable Jupiters are detected with the probability curve in Fig. 6 now representing the average fraction of the more than one day long light curve perturbation that is followed with the high time resolution photometry. Saturn mass planets will also have perturbation time scales comparable to a day and all will be assumed detected, but Uranus perturbations will have time scales comparable to the time the GC can be observed on an average night at a single southern observatory, so perhaps 75% of the detectable Uranuses may be found. These assumptions are reflected in the number of detected planets listed in Table 3.

In the second of the three models in Table 2, where both the m/M and a/R_E are invariant for each of the planets as the lens mass varies, the probabilities simply reflect the scaled values derived from Fig. 4. For example, the Jupiters in this model always correspond to a planet/lens mass ratio of 0.001 with a semimajor axis that is always about 1.3 times the Einstein ring radius when $z = 0.5$, where its probability of detection is 0.175 for a lens of any mass. Hence, the integral over the mass distribution (Eq. (9)) yields just this probability in Table 2. The detection probability is reduced somewhat for $z = 0.8$ in the table because the semimajor axis is the same as for $z = 0.5$ but the lensing zone has moved in with the Einstein ring radius leaving the Jupiters to the right of the peak in Fig. 4. Uranus at 5 AU for a solar mass star occupies the same position as Jupiter, but its probability of detection is scaled downwards by $\sqrt{m/M}$ to the appropriate value of 0.039 for $z = 0.5$ in the table. The probabilities for detecting Venuses and Earths nominally at 0.7 and 1 AU respectively (Nominally because these are the semimajor axes only for $M = 1$ in this model.) are negligibly small because these planets are always too far inside the lensing zone in this model, although one of the Earths is detected at 1 AU for $z_s = 0.8$ and few more for both $z_s = 0.5$ and 0.8 at 2.5 AU are detected.

The semimajor axes are fixed in the other two models, so the lensing zone scans the planetary positions as the lens mass is reduced. For the lower mass lenses this means that the Venuses and Earths at 0.7 and 1 AU move into the lensing zone so more are detected. More are detected when the masses are held constant because the planet/lens mass ratio increases with decreasing lens mass. All of these very close planets would be detected about stars less massive than the Sun. The detection probabilities are higher for $z_s = 0.8$ compared to $z_s = 0.5$ for the planets that are close to their central stars and lower for those further away because moving the lensing zone closer

	m_i/M, a_i ∼const.		m_i/M, a_i/R_E ∼const.		m_i, a_i ∼const.	
	$z_s = 0.5$	$z_s = 0.8$	$z_s = 0.5$	$z_s = 0.8$	$z_s = 0.5$	$z_s = 0.8$
planet	Probability of detection					
Venus	6.64×10^{-4}	1.45×10^{-3}	6.84×10^{-5}	1.30×10^{-4}	1.75×10^{-3}	3.80×10^{-3}
Earth(1)	2.31×10^{-3}	3.75×10^{-3}	2.08×10^{-4}	3.95×10^{-4}	5.92×10^{-3}	8.98×10^{-3}
Earth(2.5)	7.65×10^{-3}	7.30×10^{-3}	4.86×10^{-3}	8.37×10^{-3}	2.36×10^{-2}	1.19×10^{-2}
Uranus(5)	1.78×10^{-2}	1.14×10^{-2}	3.92×10^{-2}	3.00×10^{-2}	2.54×10^{-2}	1.55×10^{-2}
Uranus(10)	3.49×10^{-3}	1.68×10^{-3}	9.80×10^{-3}	6.29×10^{-3}	4.30×10^{-3}	1.89×10^{-3}
Jupiter	7.97×10^{-2}	5.10×10^{-2}	1.75×10^{-1}	1.34×10^{-1}	1.14×10^{-1}	6.95×10^{-2}
Saturn	8.65×10^{-3}	4.11×10^{-3}	2.40×10^{-2}	1.54×10^{-2}	1.05×10^{-2}	4.62×10^{-3}

Table 2: Detection probabilities $P(m, a, z_s)$

	m_i/M, a_i ∼const.		m_i/M, a_i/R_E ∼const.		m_i, a_i ∼const.	
planet	$z_s = 0.5$	$z_s = 0.8$	$z_s = 0.5$	$z_s = 0.8$	$z_s = 0.5$	$z_s = 0.8$
Venus	1	2	0	0	2	3
Earth(1)	2	3	0	1	5	8
Earth(2.5)	3	3	2	4	6	5
Uranus(5)	10	6	22	17	14	9
Uranus(10)	2	1	5	4	2	1
Jupiter	60	38	131	100	85	52
Saturn	6	3	18	12	8	3

Table 3: Number of planets detected.

to the lens for the higher value of z_s moves the inner planets up the rising slope of the probability curve inside the lensing zone, while moving the outer planets further down the decreasing curve outside the lensing zone.

The entries into Tables 2 and 3 identify the planets detected, but the data set obtained from the microlensing survey yields only the planet-star mass ratio and the projected position of the planet in units of the Einstein ring radius from the light curve alone. How much information about the assumed distribution of planetary masses and separations can be retrieved from the actual data set? We begin to answer this question by constructing that data set from the distributions of the stellar masses and of the projected positions of the planets. Other information about the system that can be derived from different types of observations will be neglected for the time being.

We shall develop the sample data set only for the model corresponding to the last column in Tables 2 and 3, where $z_s = 0.8$ and m_i and a_i do not change with M. To determine the likely planet/star mass ratios for the detected events, we note from Eq. (9) that the fraction of detected planets of given assumed mass and semimajor axis that orbit stars between masses $M = 0.08$ and M is given by

$$f_{_M} = \frac{\int_{0.08}^{M} \mathcal{F}(M') P(m_i, M', a_i, z_s) dM'}{\int_{0.08}^{2} \mathcal{F}(M') P(m_i, M', a_i, z_s) dM'}. \qquad (10)$$

These cumulative fractions are shown in Fig. 8 as a function of M. These fractions depend only on the planet-lens separation and not on the planetary masses, so the curves are labeled only with the semimajor axes. As mentioned earlier, the Venuses at 0.7 AU and the Earths at 1 AU are mostly detected around spectral class M stars, but the planets at 2.5 AU and beyond are distributed over a wider range of lens masses. To assign the lens mass for each of the detected planets, we spread the detected masses over the distributions shown in Fig 8 in proportion

M	m/M	r/a	r/R_E	M	m/M	r/a	r/R_E	M	m/M	r/a	r/R_E
					Venus (0.7 AU)						
0.09	2.8×10^{-5}	0.82	0.60	0.12	2.1×10^{-5}	0.95	0.59	0.20	1.3×10^{-5}	0.98	0.47
					Earth (1.0 AU)						
0.09	3.3×10^{-5}	0.71	0.73	0.14	2.1×10^{-5}	0.91	0.75	0.25	1.2×10^{-5}	0.98	0.61
0.10	3.0×10^{-5}	0.80	0.78	0.16	1.9×10^{-5}	0.94	0.73	0.40	7.5×10^{-6}	0.99	0.48
0.12	2.5×10^{-5}	0.87	0.78	0.20	1.5×10^{-5}	0.96	0.66				
					Earth (2.5 AU)						
0.14	2.1×10^{-5}	0.55	1.14	0.36	8.3×10^{-6}	0.86	1.11	0.74	4.1×10^{-6}	0.98	0.88
0.25	1.2×10^{-5}	0.75	1.17	0.49	6.1×10^{-6}	0.94	1.04				
					Jupiter (5.0 AU)						
0.12	8.3×10^{-3}	0.24	1.07	0.41	2.4×10^{-3}	0.61	1.47	0.72	1.4×10^{-3}	0.87	1.59
0.14	7.1×10^{-3}	0.29	1.20	0.42	2.4×10^{-3}	0.63	1.50	0.74	1.4×10^{-3}	0.89	1.60
0.16	6.3×10^{-3}	0.33	1.28	0.44	2.3×10^{-3}	0.64	1.49	0.77	1.3×10^{-3}	0.90	1.59
0.18	5.6×10^{-3}	0.36	1.31	0.45	2.2×10^{-3}	0.65	1.50	0.80	1.3×10^{-3}	0.91	1.58
0.19	5.3×10^{-3}	0.38	1.35	0.47	2.1×10^{-3}	0.67	1.51	0.83	1.2×10^{-3}	0.92	1.56
0.21	4.8×10^{-3}	0.41	1.38	0.48	2.1×10^{-3}	0.68	1.52	0.86	1.2×10^{-3}	0.93	1.55
0.22	4.5×10^{-3}	0.43	1.42	0.50	2.0×10^{-3}	0.70	1.53	0.90	1.1×10^{-3}	0.94	1.53
0.24	4.2×10^{-3}	0.45	1.42	0.51	2.0×10^{-3}	0.71	1.54	0.94	1.1×10^{-3}	0.95	1.52
0.25	4.0×10^{-3}	0.47	1.46	0.52	1.0×10^{-3}	0.73	1.57	0.98	1.0×10^{-3}	0.96	1.50
0.27	3.7×10^{-3}	0.48	1.43	0.54	1.9×10^{-3}	0.74	1.56	1.02	9.8×10^{-4}	0.97	1.49
0.28	3.6×10^{-3}	0.50	1.46	0.56	1.8×10^{-3}	0.76	1.57	1.07	9.3×10^{-4}	0.98	1.47
0.30	3.3×10^{-3}	0.52	1.47	0.57	1.8×10^{-3}	0.77	1.58	1.12	8.9×10^{-4}	0.99	1.45
0.31	3.2×10^{-3}	0.53	1.47	0.59	1.7×10^{-3}	0.79	1.59	1.18	8.5×10^{-4}	0.99	1.41
0.33	3.0×10^{-3}	0.54	1.46	0.61	1.6×10^{-3}	0.80	1.59	1.25	8.0×10^{-4}	0.99	1.37
0.34	2.9×10^{-3}	0.56	1.49	0.63	1.6×10^{-3}	0.81	1.58	1.36	7.4×10^{-4}	0.99	1.31
0.36	2.8×10^{-3}	0.57	1.47	0.65	1.5×10^{-3}	0.83	1.59	1.59	6.3×10^{-4}	1.00	1.23
0.38	2.6×10^{-3}	0.59	1.48	0.67	1.5×10^{-3}	0.84	1.59				
0.39	2.6×10^{-3}	0.60	1.49	0.69	1.4×10^{-3}	0.86	1.60				
					Uranus (5.0 AU)						
0.17	2.9×10^{-4}	0.34	1.28	0.43	1.2×10^{-4}	0.64	1.51	0.74	6.8×10^{-5}	0.89	1.60
0.25	2.0×10^{-4}	0.47	1.46	0.52	9.6×10^{-5}	0.72	1.55	0.93	5.4×10^{-5}	0.95	1.52
0.34	1.5×10^{-4}	0.56	1.49	0.61	8.2×10^{-5}	0.81	1.61	1.22	4.1×10^{-5}	0.98	1.37
					Saturn (10.0 AU)						
0.54	5.6×10^{-4}	0.33	1.39	0.74	4.1×10^{-4}	0.60	2.16	1.11	2.7×10^{-4}	0.93	2.73
					Uranus (10.0 AU)						
				0.74	6.7×10^{-5}	0.72	2.59				

Table 4: Probable distributions of planet/star mass ratios and separations

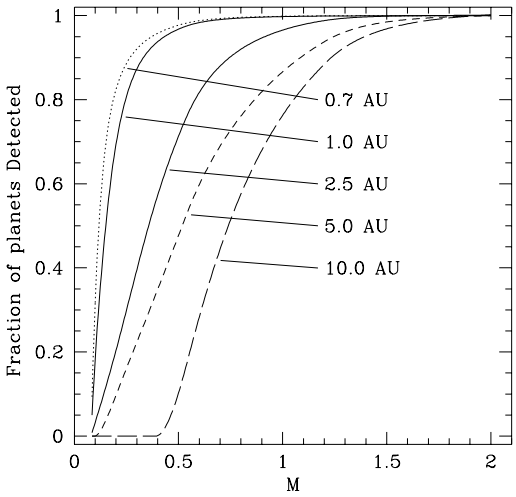

Fig. 8.— Fraction of planets detected in the mass range 0.08 to M for each semimajor axis in the model planetary systems. Close planets are preferentially detected around the lower mass stars, whereas, the more distant planets are detected over a wider range of masses.

to the fraction detected in each range. For example, from Table 3 the last column shows that about three Venuses would have been detected. From Fig. 8, about 1/3 of the detected planets should be found about lenses in the mass range $0.08 < M < 0.10$, another third in $0.10 < M < 0.14$ and the remaining third in $M > 0.14$. We can assign the probable lens masses for the Venus detections such that there is one within each range of masses corresponding to 1/3 of the probable detections. If we choose these to correspond to values of the cumulative fraction of detections near 1/6, 1/2, 5/6, the lens masses about which the Venuses are detected would be 0.09, 0.12, 0.20 respectively from Fig. 8. We can systematically assign lens masses to N detected planets with a particular semimajor axis by choosing those values of M where the cumulative fraction of probable detections in Fig. 8 is $1/(2N) + k/N,\ k = 0, 1, \cdots N-1$ as was done for Venus. The results of this exercise are shown in Table 4.

The determination of the distribution of normalized projected separations is more involved and not so well constrained as that for the planet/star mass ratios. An Earth with $a = 2.5AU$ at its extreme projected separation would be inside R_E for a large star, but outside R_E for a small star. But this Earth, uniformly distributed on a sphere of radius a, could be at any projected separation from the lens less than a with a probability distribution given by $p(r)dr$ in Eq. (3). For a particular lens mass M with a planet at a particular semimajor axis a, the probability of *detecting* the planet in a range Δr about $r < a$ is the probability of *finding* the planet in this range weighted by the probability of detecting the planet at that particular separation. The first probability peaks at $r = a$ and the second peaks near the Einstein ring radius for the point sources considered here. Although the probability distribution $P(m, a, M, z_s)$ obtained by scaling and shifting the curve in Fig. 4 has been averaged over the line of sight for a model distribution of stars, we can use it as an approximation to the second probability by replacing a by $r < a$. It peaks near the Einstein ring radius and should give a reasonably good representation of the proper weighting of the projected distance probability. The fraction f_d of planets of mass m, semimajor axis a that would be detected in the range $0-r$ about an ensemble of lenses of mass M, average fractional distance z_s is thus

$$f_d(r) = \frac{\int_0^r p(r')P(m, r', M, z_s)dr'}{\int_0^a p(r')P(m, r', M, z_s)dr'}. \qquad (11)$$

In Fig. 9 $f_d(r)$ is shown for intermediate values of the lens mass M in the lens mass distribution assigned to each planet type. Three Venus mass planets are detected in our model data set about lenses with masses 0.09, 0.12 and $0.20M_\odot$ with corresponding Einstein ring radii of 0.97, 1.12, 1.44 AU respectively calculated at the average distance $z_s = 0.8$. The curves for the extreme values of M for Venus in Fig. 9 almost coincide with that for the intermediate value shown for $M = 0.12$. We therefore distribute the distances of the detected Venuses according to this curve (like the distributions of lens masses) at values of $r/a = 0.82, 0.95, 0.98$ corresponding to $f_d(r) \approx 0.16, 0.5, 0.83$ respectively. We assign the closer planets to the smaller lenses since the closer proximity of the Einstein ring radii increases their probability of detection. The values of r/a and r/R_E are given in Table 4.

The other planet types are treated in the same way with the separations being distributed according to $f_d(r)$ for a lens mass giving a curve approximately midway between the curves for the extreme values

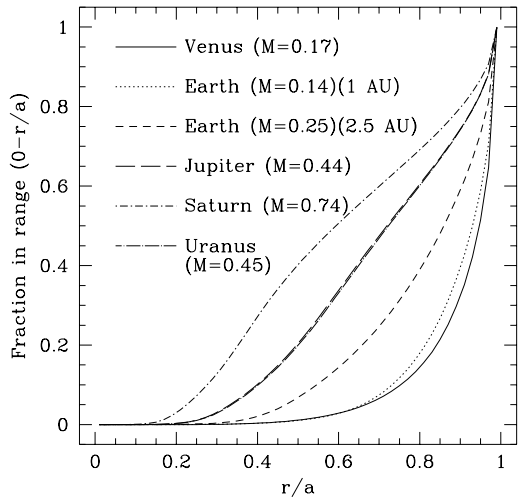

Fig. 9.— Fraction of planets detected in range 0 to r/a for each planetary type in the model systems. Curves for each planet type correspond to a lens mass near the mean value of the distribution of lens masses about which that planet type were found in Table 4. They are the basis for the assigned distribution in projected separations of planets.

of the lens mass in the distribution. Here again the smallest separations are associated with the smallest lenses with the values given in Table 4. As the semimajor axis gets small compared to the Einstein ring radius the distribution is dominated by the probability of the projected separation of the planet which peaks at $r = a$. The effect of the higher probability of detection at the Einstein ring radius becomes important as the projected separation approaches this radius and beyond. Hence, we find that $f_d(r)$ for all the planet types moves toward the Venus curve when the lens mass is large. For the Earths at 1 AU at the largest lens mass $M = 0.40$, about which one of these closer Earths was detected, $f_d(r)$ almost coincides with the Venus curve. For the Earths at 1 AU, the values of r/a and r/R_E (at $z_s = 0.8$) in Table 4 are distributed according to the curve for $M = 0.14$. Similarly, the Earths at 2.5 AU are assigned separations according to the distribution for $M = 0.25$, Jupiters according to the distribution for $M = 0.44$, Saturns according to the distribution for $M = 0.74$, and Uranuses at 5 AU according to the distribution for $M = 0.45$. The single Uranus that was detected at 10 AU is placed at $r/a = 0.72$ corresponding to $f_d(r) = 0.5$ for $M = 0.74$. This procedure gives a reasonably probable distribution of separations, since the larger fraction detected at smaller distances for smaller lenses is accounted for by assigning the closer planets to the smaller lens masses.

The values of m/M and r/R_E in Table 4 comprise the information about the detected planets that can be learned from the light curve. Although additional information can be obtained by further observations of a different type, we start by seeing what can be deduced about the planetary systems from this information alone.

6. Interpretation and discussion

One of the first things that one notices about the data set in Table 4 is that the mass ratios for the detected planets are reasonably good signatures for the actual masses of the planets in spite of the varying lens masses. This results from the fact that the lens masses only span an order of magnitude whereas the planetary masses span three orders of magnitude. We would thus conclude that statistically $m/M \sim 10^{-5}$ corresponds to terrestrial mass planets, $m/M \sim 10^{-4}$ to Uranus mass planets and $m/M \sim 10^{-3}$ to Jupiter mass planets, where the terms terrestrial, Uranus and Jupiter are meant to constrain the masses only to about an order of magnitude from the least to the most massive in each designation. This grouping is evident in Fig. 10 where we have plotted the values of m/M *vs* r/R_E. We also notice that the lower mass planets tend to fall inside the Einstein ring radii of their respective lenses, whereas the higher mass planets tend to fall outside. Thus, this solar system characteristic of our original assumptions is recovered. The concentration of the lower mass planets near $r/R_E \approx 1$ are the Earths at 2.5 AU, and we could infer this approximate location for these planets from the fact that the probability of detection is highest when the planets have semimajor axes near the Einstein ring radius and that radius is near 2.5 AU for the dominant number of small mass stars in the distribution. The concentration of the medium and high mass planets near $r/R_E = 1.5$ is also striking, but this reflects the fact that these planets have semimajor axes that are larger than the Einstein rings of nearly all likely lenses, but have a greater probability of being detected if their projected separations

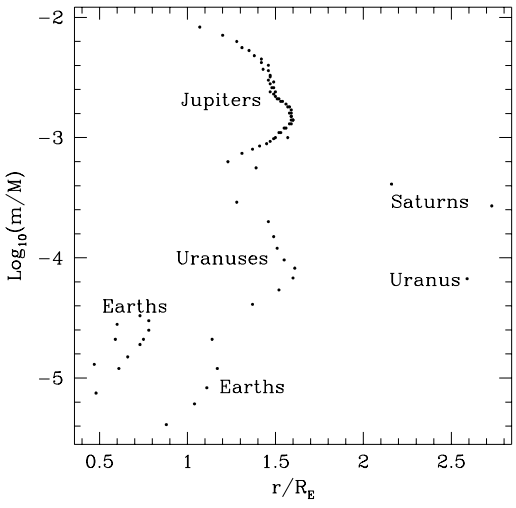

Fig. 10.— Planet/lens mass ratios as a function of the projected separation for the constructed data set in Table 4.

are closer to the Einstein ring radius. Two Saturns and the single detected Uranus at 10 AU comprise the three points with $r/R_E > 2$.

The facts that all the sources will not be 8 kpc from the Sun and that the masses of real planets will not be limited to a few discrete values would introduce additional scatter into the data set displayed in Fig. 10. The groups would no longer be evident, although the general trend of the distribution of points would still prevail if other planetary systems were to have small planets close to their stars and larger planets further away. The very close large planets around 51 Peg and 55 Cnc within .05 to .1 AU could not be detected, but the very large planet about 47 UMa at 2.1 AU, if detected, would yield a point in Fig. 10 most likely between values of r/R_E between 0.4 and 0.5 and $m/M > 2.5 \times 10^{-3}$ ($m \sin i = 2.5 \times 10^{-3} M_\odot$). If many points were found in this region of Fig. 10, it would imply the common existence of large planets considerably closer to their central stars than those in the solar system.

The detection of sixteen planets with planet/lens mass ratios near 10^{-5} would imply that such planets are relatively common given the low probability of their detection. However, care must be exercised in inferring the fraction of lenses having planets of various masses from the number of planets detected and the probabilities of detection, since the latter are dependent on the assumptions about the planetary distributions and the lens mass function. For example, with the same mass function, we detected respectively 8, 5 and 16 terrestrial type planets for $z_s = 0.8$ for the three models, implying that our estimate of the fraction of lenses having terrestrial mass planets could not be constrained by less than a factor of 2. Even though a factor of 2 may not sound too bad, the small number of terrestrial planet detections makes such statistics suspect. In any case the model dependence of the interpretation is just as severe as that in deriving the expectations from the search. All the terrestrial planets are detected about stars considerably less massive than the Sun except higher mass lenses can be inferred for the terrestrial planets detected with r/R_E near 1.

The determination of the fraction of lenses having Jupiters is similarly uncertain by at least a factor of 2. However, if nearly all of these would correspond to values of $r/R_E > 1$ as in our one data set, we could infer the Jupiters to be relatively far away from their stars consistent with formation near the ice condensation point in the pre-planetary nebula. This consistency with the current paradigm of planet formation in the solar system and the inferred non dominance of giant planet migration (Ward and Hourigan, 1989; Lin, *et al.* 1996; Ward, 1996) in planetary system histories allows us the further inference of the existence of several terrestrial type planets inside the Jupiter orbit, even though the latter were not directly detected. The massive planets close to their primaries can be detected by radial velocity and astrometric techniques on the relatively short time scales of the orbit periods as already demonstrated. Statistics for massive planets in Jupiter-like orbits would be delayed in such surveys, but would start accumulating immediately in an intensive microlensing search. An occasional detection of a low mass planet would support the inference that where there are Jupiters far out, terrestrial planets are in close.

The detection of the nine Uranus mass planets just outside the Einstein Ring radii in Table 4 and Fig. 10 would imply that the Jupiters are not there for these systems. A further inference could be that a relatively larger number terrestrial type planets may be inside 5 AU for those particular stars than exist in our own solar system (Wetherill, 1994). The ratio of the number of Uranuses to the number of Jupiters in such a

data set would test the implication of current theories that Jupiters at distances where they could form in the nebula may be even more rare than we assumed at the outset. Radial velocity and astrometric surveys can determine in a relatively short time if many Jupiters have migrated to or are otherwise positioned close to their stars.

We see that several conclusions can be drawn from the statistics of the planet/star mass ratios and projected separations obtainable from the microlensing light curves alone. The fraction of the stars that have planets of various masses in their lensing zones can be estimated. However, the model dependence of the interpretation of these data limits the accuracy of the estimates to no better than a factor of 2. The planet/star mass ratios inferred from the data are reasonably good indicators of the actual planetary masses because of the limited range of likely stellar masses. A rough dependence of the planet-star separation on the planetary mass may be inferred from a plot of r/R_E *vs* m/M (Fig. 10). The number of Uranuses detected where Jupiters might be expected constrains the success rate for the Jupiter-forming process.

Few of the terrestrial type planets that are detected will be close enough to their stars for habitability. Recent developments indicate that a way to infer the frequency of such planets may be the distribution of separations of the massive planets from their stars. About 1 in 30 stars in radial velicity surveys to date seem to have giant planetary mass objects close to their primaries (W. Cochran, private communication 1996). There are several theoretical arguments showing how Jupiters could be removed from their region of formation and, in some cases, account for the close planets. These include torques from spiral density waves in a persistent nebula generated by fully formed planets (Lin *et al*, 1996), by planetary billiards among giant planets formed too close together for stabilty (Rasio and Ford, 1996, Weidenschilling and Marzari, 1996) or by rapid migration of the solid body accretional cores toward the star before acquisition of the gaseous envelopes (Ward and Hourigan, 1989; Ward, 1996).

The observations and the theories that attempt to account for them imply that most of the material that would have gone into terrestrial type planets could have been eliminated through interactions with the giant planets or their cores that invaded the terrestrial planet territory. Therefore, the greatest contribution that a microlensing search for planets may make may be to determine where the giant or subgiant planets are relative to their central stars. The absence of many Jupiters or Uranuses detected outside the Einstein ring radii of their central stars may indicate that terrestrial-type planets in habitable zones are infrequent. On the other hand, finding most of a reasonably large number of massive planets relatively far from their stars would indicate that the scattering or migration mechanisms did not dominate planetary system histories and may give a better inference of the frequency of occurence of terrestrial planets than that provided by the meagre statistics of the latter's direct detection.

We have limited the discussion so far to just what may be learned from the statistics of the microlensing light curves, since that is the only information that would be systematically obtained in the microlensing search described above. More information can be obtained about an individual system with additional observations. If the lens can be spectrally classified, the actual masses of the planets of such lenses can be obtained. Although spectral classification allows an estimate of the distance D_{OL} to the lens from the known luminosity and estimates of interstellar extinction, the additional unknown D_{OS} in R_E limits the accuracy with which the actual separation between lens and planet can be determined. An isolated star with visual magnitude $m_v = 24$ can be spectrally classified with a Keck telescope (R.M. Rich, private communication, 1996). In the crowded field toward the galactic center we should at least be able to classify a star with $m_v = 22$, which corresponds to a K5V main sequence dwarf at the galactic center. The time after the event that one must wait in order to separate the light of the lens from that of the source depends on the rate of development of interferometric techniques, but we would know the masses of those planetary companions of lenses earlier than K5V. The mass of a K5V star is about $0.69M_\odot$ (Allen, 1973), so the remaining lenses of later spectral type have a masses ranging over a factor of 8.

This is not that great an advantage since only about 25% of the lenses in Table 4 have $M > 0.69$. Still, masses of nearly all of the detected planets would be known to within about a factor of 3 (an order of magnitude from the least to the highest mass estimate) from a microlensing search, and the projected separations in terms of the Einstein ring radii would yield estimates of the actual separations. In

some circumstances observations using effects of differential limb darkening of finite sized sources (Gould and Welch, 1996) or of limb brightened H-K lines of Calcium (Loeb and Sassalov, 1995) as a small planetary Einstein ring traversed the source might be used to gain additional information about the lens system. However, discussion of the practical aspects of incorporating such observations into an intensive microlensing survey should await inclusion of the effects of finite sized sources in the detection of small planets in an analysis like that above. Inclusion of the finite source size effects in a development similar to the above must await the accumulation of an array of detection probability curves like those of Bennett and Rhie (1996) covering a range of parameters. A possible approach to small planet detection with finite sized sources is outlined in the next section.

7. Finite sized sources

Allowing for the finite size of the source changes the procedure used to determine the planet/lens mass ratio for small planets, since the time scale of the planetary perturbation is now extended beyond the transit time of a point source across the Einstein ring of the planet by the finite angular size of the source star. The maximum amplitude of the perturbation of the light curve is also reduced since a small planet can amplify only a fraction of an extended image. The determination of the probability of a planetary detection (Bennett and Rhie, 1996) during an event is much different from that developed analytically by Gould and Loeb (1992). The Bennett and Rhie technique will be described below, and an example calculation of averaging a Bennett and Rhie detection probability over the stellar mass function establishes a procedure for determining the overall probability of detecting small mass planets. Even though this more correctly determined detection probability for small mass planets has little to do with that determined by scaling the Gould and Loeb probability curve for point sources, their remarkably close agreement for this one example implies that our conclusions above for the overall probability of detecting small mass planets may not be in error by more than a factor of 2.

As pointed out above, the finite size of the source star must be taken into account when the Einstein ring angular radius of the planet becomes comparable with the angular size of the source star. The angular size of a star at 8 kpc is $\theta_* = 6 \times 10^{-7} R_*/R_\odot$ arcsec, whereas the Einstein ring radius of a planet for a source at 8 kpc is $1 \times 10^{-3}\sqrt{m(1-z)/(M_\odot z)} = 2\times10^{-5}$ arcsec for a Jupiter at 6 kpc and 1×10^{-6} arcsec for an Earth at 6 kpc. So only for the largest super giants will the perturbation by a Jupiter mass planet show the effects of the finite size of the source, but essentially every perturbation by an Earth mass planet will be greatly affected by the source size. Bennett and Rhie (1996) determine detection probabilities for planet-star mass ratios of 10^{-5} and 10^{-4} for values of z of 0.5 and 0.8 with source radii of $R_* = 3$ and $13R_\odot$. We show how these probabilities can be averaged over the mass function, but that the probability determinations must be extended over the parameter space before rigorous overall probabilities of detection of Earth mass planets can be found for the finite sized sources.

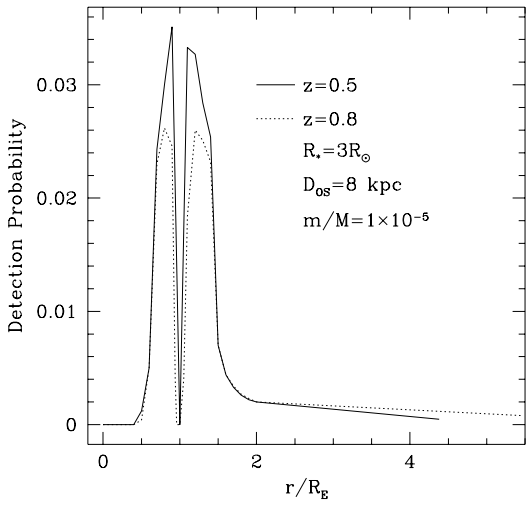

Fig. 11.— Probability of detecting a planet as a function of the projected lens-planet separation when $m/M = 10^{-5}$ and the source star at the center of the galaxy has a radius of $3R_\odot$. (after Bennett and Rhie, 1996). The Bennett and Rhie curves have been extended beyond $r = 2R_E$ by determining the probability of detecting a distant, essentially isolated planet given that the planet's central star has acted as a lens.

Fig. 11 shows the Bennett and Rhie (1996) probabilities of detecting a planet with $m/M = 10^{-5}$ (an Earth mass when $M = 0.3$) for the two lens distances

as a function of the planet's projected separation from its central star when the source star at the center of the galaxy has a radius of $3R_\odot$. This radius is a little larger than the peak in the distribution of radii of main sequence turn-off stars in the galactic bulge (Loeb and Sasselov, 1996). The probabilities are determined by numerically calculating many light curves for a set of impact parameters of the source relative to the lens spanning the Einstein ring of the lens and for all orientations of the source trajectory across the ring relative to the lens-planet line. The fraction of the light curves that displayed a perturbation more than 4% of the unperturbed amplification for more than 1/400 of the time scale of the entire event gives the probability of detection. The effect of the finite sized source is shown dramatically by the strong dip in the detection probability when the projected separation of the planet is near the Einstein ring radius. A point source yields a maximum detection probability of detection when the planet is very near the Einstein ring radius. This behavior for the finite sized source follows because the image is spread out to its maximum size when it is near the Einstein ring radius and the planet can focus only a much smaller fraction of the image light—failing to reach threshold detection. It is of interest to note that the maximum probability of detection for $z = 0.5$ is approximately double the maximum scaled probability for the point source case of Gould and Loeb (1992) (0.034 *vs.* 0.017 for $m/M = 10^{-5}$), although the latter would be increased somewhat if 4% instead of 5% were used as the detection criterion. The Bennett and Rhie detection probability falls somewhat for $z = 0.8$ because the Einstein ring radius of the planet is reduced at the larger value of z so a smaller fraction of the source image is amplified by the planet for similar geometries.

Below we shall average these probabilities over the mass function of the lenses for planet orbital semimajor axes 0.7, 1.0, 2.5 and 5 AU respectively. The largest semimajor axis corresponds to a separation of $5.5R_E$ for $M = 0.08$ and $z = 0.8$. We have therefore extended the Bennett and Rhie curves from $r = 2R_E$ to $5.5R_E$ by estimating the probabilities of detecting the distant planet (Appendix B).

The functional dependence of the probability curves is $P = P(m, M, R_*, z, r)$, where r is the projected separation of the planet from the lens in the lens plane and R_* is the radius of the source (assumed to be at 8 kpc distance). The probability of detecting a planet of mass m with semimajor axis a during an event with source radius R_*, lens of mass M located at fractional distance z is the probability of finding the planet at projected distance between r and $r + dr$ (Eq. (3)) times $P(m, M, R_*, z, r)$ integrated from 0 to a or

$$P(m, M, R_*, z, a) = \int_0^a \frac{P(m, M, R_*, z, r) r dr}{\sqrt{1 - \frac{r^2}{a^2}}}, \quad (12)$$

where all distances are determined in terms of the Einstein ring radius. So in general the integral is a function of M for given m, R_*, z, a. If the probability curves are left in the broken line form shown in Fig. 11, each linear segment substituted into Eq. (12) is analytically integrable and the singularity in the integrand at $r = a$ is removed. Similar to the Gould and Loeb probabilities, the probability of detecting a planet of mass m with semimajor axis a as a companion of a lens at z in an event with source radius R_* averaged over the event mass distribution is

$$P(m, R_*, z, a) = \int_{0.08}^{2} \mathcal{F}(M) P(m, M, R_*, z, a) dM, \quad (13)$$

The curves in Fig. 11 correspond to a particular mass ratio, so we can only evaluate the averaged probability in Eq. (13) for the case where the planet/star mass ratio is fixed at this particular value as the lens mass varies. These probabilities are shown in Table 5 along with those for point sources. With the exception of $a = 0.7AU$, the probabilities for point and finite sources are remarkably close. However, we cannot draw any inferences from these comparisons except perhaps to think that the probabilities for detecting Earth mass planets when point sources are assumed are closer to the real values than we might have expected. The finite source probabilities must be averaged over the distribution of lenses along the line of sight and over the distribution of sizes of those sources that will be monitored in any microlensing survey. This requires the generation of curves like those in Fig. 11 for a sufficient number of source sizes and lens distances for reasonable interpolation over the distributions. In addition, if we were to consider the model where the mass of the planet is held constant instead of the mass ratio, detection probability curves must be generated for various mass ratios. Hence, more accurate estimates of the detection of Earth mass planets through microlensing must await generation of this array of Bennett and Rhie type probability curves or, as may be unlikely,

	$P(m, R_*, z, a)$ (Eq. (13))		$P(m, a, z_a)A$ (Eq. (9))	
a AU	z=0.5	z=0.8	z=0.5	z=0.8
0.7	0.000155	0.000992	0.00133	0.00289
1.0	0.00239	0.00405	0.00421	0.00685
2.5	0.0158	0.0121	0.0140	0.0133
5.0	0.0105	0.00592	0.00797	0.00510

Table 5: Probabilities of detecting a planet with $m/M = 10^{-5}$ and $R_* = 3R_\odot$ with probabilities derived for point sources with m/M fixed at 10^{-5} included for comparison

a clever scheme of avoiding the lengthy calculations can be contrived. On the other hand, the comparison of the probabilities in Table 5 with those from the point source calculations, may indicate that our estimates in Tables 2 and 3 for the Earth mass planets are correct to within a factor of 2.

For the point source, the planet only perturbs the single lens light curve significantly when it is within a planetary Einstein ring radius of one of the unperturbed image positions in the lens plane. If the angular size of this Einstein ring is small compared with that of the source star, it will be small compared with the size of the image in the lens plane. Nothing much happens as the planetary Einstein ring approaches the edge of a large image, since it can amplify only a small fraction of the image light. That fraction of course depends on the angular size of the image (or angular size of the source star) compared to that of the planetary Einstein ring, so bigger perturbations occur for smaller sources. Generally, a significant perturbation occurs only as the planetary Einstein ring moves well into the finite image, which occurs, at least for a planet outside the lens Einstein ring radius, as the caustic curve in the source plane moves across the face of the source star. The picture is more complicated if the planet is inside the lens Einstein ring radius since there are two caustics giving positive amplification separated by a deep negative trough, If the finite sized source covers both caustic and negative trough, the resulting cancellation can keep the total amplification undetectably small (Bennett and Rhie, 1996). If the source angular diameter is less than the separation of the two caustics a negative perturbation of the light curve can be detected for the inside planet.

In most cases the perturbation of the light curve will have more structure than that shown by the example of Fig. 3, since regions of positive amplification are always interleaved with regions of negative amplification. Examples of such light curves for several planet/lens mass ratios, several geometries and several source sizes are shown by Bennett and Rhie (1996) and by Wambsganss (1996). The perturbation light curve structure is most pronounced when the source size is smaller than the caustic in the source plane, but persists if the source is not too large, where a typical pattern is a negative perturbation surrounded by smaller positive perturbations for a planet inside the Einstein ring of the lensing star and a positive perturbation surrounded by smaller negative perturbations for a planet outside the Einstein ring (Bennett and Rhie, 1996).

The structure of the light curve perturbation complicates the simple picture of determining the planet/lens mass ratio from the ratio of the perturbation time scale and the event time scale, but at the same time supplies sufficient constraints for a more precise determination of that mass ratio. The normalized impact parameter of the lens-source encounter is known from the maximum of the light curve, and the angle at which the source encounters the lens-planet line and the location of the unperturbed images of the source are known from the position of the perturbation on the light curve. The projected position of the planet must be near one of the unperturbed images in order effect the perturbation. The selection of the correct image is usually very easy with a well sampled light curve as noted above (Gaudi and Gould, 1996). The planet may pass either side of the image and create the same maximum perturbation, but with different symmetries in the wings of the light curve that are nearly always discernable for passage near the image inside the Einstein ring (minor image) and usually discernable for passage near the outside image (major image) with 1% photometry and good coverage

(Gaudi and Gould, 1996). If the ratio of the source angular radius to the angular radius of the planetary Einstein ring is not too large, a condition satisfied by Earth mass planets when the source is a turn-off main sequence star at the center of the galaxy ($R_* \sim 2\,\mathrm{to}\,3R_\odot$), the remaining uncertainty in the projected position of the planet is negligibly small. As the angular size of the source is known spectroscopically from the apparent brightness and an estimate of interstellar absorption, the planet/star mass ratio, as the remaining free parameter, can be adjusted to match the light curve and thereby constrain its value quite well. A model of limb darkening and slight adjustments in the source trajectory through the lens-planet system may be necessary to refine the determination.

About 25% of the events toward the galactic center will involve so-called clump giants ($R_* \sim 13R_\odot$) as sources (Alcock, *et al* 1996). Gaudi and Gould (1996) call attention to a potentially serious uncertainty in the planet/star mass ratio by demonstrating a set of similar, low amplitude perturbation light curves involving the major image with the same maximum change in amplification and the same full-width-half-maximum of the main part of the perturbation but corresponding to an order of magnitude range of planet/star mass ratios. The uncertainties are reduced to acceptability with good coverage of both wings of the light curves with 1% photometry. However, the practical difficulties in getting such coverage routinely means that the uncertainties would remain for many of these events. One means of reducing the uncertainties in the mass ratio to acceptable values offered by Gaudi and Gould is to distinguish the curves with simultaneous photometry in the infrared and optical. Giant stars are less limb darkened in the infrared than in the optical, and the distinct color effects of the event can select the proper mass ratio. On the other hand, the planetary perturbations are more difficult to detect in the first place with giant sources because of the lower amplitude of the perturbations. In most of the cases were the uncertainty would be severe, the observing strategy used by Bennett and Rhie (1996) would have failed to detect the planet (D. Bennett, private communication 1996). This would eliminate most of the cases where the uncertainty in m/M was excessive from the data set. But even with those that remain, there are ways to determine both m/M and the projected separation to sufficient accuracy (Gaudi and Gould, 1996).

So the effect of finite source size will not hinder the determination of the planet/lens mass ratio or the normalized projected separation of the planet from the lens. It thus makes sense to pursue the exercise outlined above to determine the overall probability of detection of small mass planets when the finite source size is accounted for. In the meantime, we can take some assurance from the comparison of the detection probabilities for finite and point sources in Table 5, that our estimates for the detection of small planets may be within a factor of 2 of those that will be derived for the finite sources.

We end by cautioning the reader to keep in mind the severe assumption dependence of the expectations for planet discoveries in any microlensing search. (Table 3 gives approximately 56, 138, or 81 planets detected for the three sets of assumptions assuming that no planets are found about members of binary star systems.) But he or she should also keep in mind that the detection scheme is robust with simple, ground based technology, and that if they are there, the planets will be detected with useful bounds placed on their masses and planet-star separations with a data set based on the light curves alone. Finally, although microlensing is the only ground based scheme that is sensitive to Earth-mass planets, finding most of a large number of giant or semi-giant planets beyond the Einstein ring radii of their stars may be a better indicator of the frequency of occurrence of terrestrial planets than the few of the latter that are directly detected.

Appendices

A. Analytic Representation of the Gould and Loeb (1992) detection probability curve

$$x = \frac{0.25a}{\sqrt{M}}\sqrt{\frac{0.25}{z(1-z)}}$$

$$\begin{aligned} P &= 0, \qquad 0 \le x \le 0.1 \\ &= 0.001763066\left[e^{7.6653342*(x-0.1)} - 1.0\right], \\ &\quad 0.1 \le x \le 0.564 \\ &= 0.4733727x - 0.2069822, \qquad 0.564 \le x \le 0.733 \end{aligned}$$

$$= -84.9463918x^4 + 286.1509291x^3 - 361.2286639x^2 + 202.6160685x - 42.4667434, \quad 0.733 \le x \le 0.9$$

$$= 0.0475524d0 * x + .1204028, \quad 0.9 \le x \le 1.043$$

$$= -1.3858063x^4 + 6.0121987x^3 - 9.8567924x^2 + 7.2772186x - 1.8790527, \quad 1.043 \le x \le 1.4$$

$$= -0.1806818x + 0.4164545, \quad 1.4 \le x \le 1.664$$

$$= 0.02869257x^4 - 0.3053152x^3 + 1.23616560x^2 - 2.2872802x + 1.6857629, \quad 1.164 \le x \le 3.0$$

$$= -0.015d0 * x + 0.075, \qquad 3.0 \le x \le 5.0$$

$$= 0, \qquad x \ge 5.0$$

B. Probability of detection of a planet that is far from its central star

Bennett and Rhie (1996) require an amplification of 1.58 before a microlensing event is to be followed with high time resolution photometry in search of a planet. This requires that the source have an impact parameter relative to the lens of less than 0.7637 according to Eq. (2). A distant planet ($a >> R_E$) will act as a solitary lens for most of its probable projected distances from the lens. The planetary Einstein ring radius R_{E_p} is small compared to the projected radius of the source star, which requires that the planet actually traverse the face of the source star for significant amplification. (This compares with its having to traverse the image of the source star for significant amplification when it is close to its central star.) The maximum amplification is found by aligning the planet with the center of the source, multiplying Eq. (2) by an element of area of the source (normalized by the Einstein ring radius) integrating over the total area of the source and dividing by the area. This yields

$$A_{max} = \sqrt{1 + \frac{4\theta^2_{R_{Ep}}}{\theta^2_*}},$$

where $\theta_{R_{Ep}}$ is the angle subtended by the Einstein ring radius of the planet and θ_* is that subtended by the source radius R_*. For the mass $10^{-5} \times 0.08 M_\odot$ with $R_* = 3R_\odot$, $A_{max} = 1.60$ for $z = 0.5$, and $A_{max} = 1.125$ for $z = 0.8$. In both cases the planet would be detected by the 4% criterion, but only after the event because of the $A = 1.58$ threshold before a planet is sought. These maximum amplifications also show why it is necessary for the planet to be on the disk of the source star before detection is possible.

The planet must be within the swath that is $2 \times .7637 R_E$ wide and $2a$ long centered on the lens star to have a chance of being intercepted by the source during the event. However, since the distant planet can be detected only after the event, we only consider the probability P_s that the planet is in one half of this swath.

$$P_s = \frac{1}{2}\int_0^R \frac{r\,dr}{a^2\sqrt{1 - r^2/a^2}} + \int_R^a dr \int_{-\sin^{-1}R/r}^{\sin^{-1}R/r} \frac{r}{a^2\sqrt{1 - r^2/a^2}} \frac{d\theta}{2\pi}$$

$P_s = 0.0494$ for $z = 0.8$ where the swath is $2 \times 0.915 \times 5\,(\mathrm{AU})^2$, and $P_s = 0.0635$ for $z = 0.5$ where the swath is $2 \times 1.14 \times 5\,(\mathrm{AU})^2$.

For $z = 0.8$, $3R_\odot$ projected onto the lens plane and divided by R_E for $M = 0.08$ is $r_* = 0.0122$. If the planet is within the swath area it is approximately uniformly distributed in the direction perpendicular to the long axis of the swath. The probability that the source will encounter the planet is then $r_*/0.7637 = 0.016$ and the probability of detection is this probability times the probability that the planet is within the swath or 0.00079. This establishes the point (5.46,0.00079) to which the Bennett and Rhie graph for $z = 0.8$ is extended in Fig. 11. For $z = 0.5$, $r_* = 0.00614$, the probability of interception is 0.00803 and probability of detection is 0.00051. So the Bennett and Rhie graph for $z = 0.5$ is extended to the point (4.37, 0.00051) in Fig. 11.

Acknowledgements

I am very grateful to E. Agol, D. Bennett, O. Blaes, A. Gould, A. Loeb and S. Rhie for reading a draft of the manuscript, pointing out some errors and offering suggestions for improving the presentation. I especially thank A. Gould and A. Loeb for their support over the last year, while I studied the art of the

microlensing detection of planets. Special thanks are due David Tytler who motivated a concentrated effort toward microlensing planet detection. This work was supported by the NASA PG&G program under grant NAGW 2061.

References

Alard, C., S. Mao, and J. Guibert (1995) Object DUO 2 - a new binary lens candidate, *Astron. Astrophys.* **300**, L17-L20.

Alcock, C., R.A. Allsman, T.S. Axelrod, D.P. Bennett, K.H. Cook, K.C. Freeman, K. Griest, S.L. Marshall, S. Perlmutter, B.A. Peterson, M.R. Pratt, P.J. Quinn, A.W. Rodgers, C.W. Stubbs, and W. Sutherland (1995) Probable gravitational microlensing toward the galactic bulge, *Astrophys. J.* **445**, 133-139.

Alcock, C., R.A. Allsman, T.S. Axelrod, D.P. Bennett, K.H. Cook, K.C. Freeman, K. Griest, J. Guern, M.J. Lehner, S.L. Marshall, H.-S Park, S. Perlmutter, B.A. Peterson, M.R. Pratt, P.J. Quinn, A.W. Rodgers, C.W. Stubbs, and W. Sutherland (1996) The Macho project: 45 candidate microlensing events from the first year of galactic bulge data, *Astrophys. J.* In Press.

Allen, C.W. (1973) *Astrophysical Quantities*, Althone Press, U. of London, p 209.

Basu, S. and N.C. Rana (1992) Multiplicity-corrected mass function of main-sequence stars in the solar neighborhood, *Astrophys. J.* **393**, 373-384.

Beichman, C. A. (Ed.) (1996) *A Road Map for the Exploration of Neighboring Planetary Systems*, Jet Propulsion Lab Publication 92-22, Pasadena, CA.

Bennett, D.P. and S.H. Rhie (1996) Detecting Earth-mass planets with gravitational microlensing, *Astrophys. J. Let.* In Press.

Boss, A.P. (1996) Giants and dwarfs meet in the middle, *Nature* **379**, 397-398.

Butler, R.P. and G.W. Marcy (1996) A planet orbiting 47 UMa, *Astrophs. J. Let.* In Press.

Chang, K., and S. Refsdal (1979) Flux variations of QSO 0957+561A,B and image splitting by stars near the light path, *Nature* **282**, 561.

Feller, W. (1957) *An Introduction to Probability Theory and its Applications*, John Wiley and Sons, New York.

Gatewood, G. (1996) Lalande 21185, *Bull. Amer. Astron. Soc.* **28**, 885.

Gauli, B.S. and A. Gould (1996) Planet parameters in microlensing events, *Astrophys. J.*, Submitted.

Gould, A. (1996) Microlensing and the stellar mass function, *Proc. Astron. Soc. Pac.* In press.

Gould, A. and D.L. Welch (1996) Macho proper motions from optical/infradred photometry, *Astrophys. J.* **464**, 212-217.

Gould, A., and A. Loeb (1992) Discovering planetary systems through gravitational microlenses, *Astrophys. J.* **396**, 104-114.

Lin, D.N.C., P. Bodenheimer and D.C. Richardson (1996) Orbital migration of planetary companion of 51 Pegasi to its present location, *Nature* **380**, 606-607.

Loeb, A. and D. Sassalov (1995) Removing Degeneracy of microlensing light curves through narrowband photometry of giants, *Astrophys. J. Let.* **449**, L33-L36.

Mao, S. and B. Paczyński (1991) Gravitational microlensing by double stars and planetary systems, *Astrophys. J.* **374**,L37-L40.

Marcy, G.W. and R. P. Butler (1996) A planetary companion to 70 Vir, *Astrophs. J. Let.* In Press.

Mayor, M. and D. Queloz (1995) A Jupiter-mass companion to a solar-type star, *Nature* **378**, 355-359.

Mazeh, T., M. Mayor and D.W. Latham (1996) Eccentricity vs. mass for low-mass companions and planets, Submitted.

Rasio, F.A. and E.B. Ford (1996) Dynamical instabilities and the formation of extrasolar planetary systems, *Science* **274**, 954-956.

Schneider, P., and A. Weiss (1986) The two-point-mass lens: detailed investigation of a special asymmetric gravitational lens, *Astron. Astrophys.* **164**, 237-259.

Strom, K.M., J. Kepner, S.E. Strom (1995) The evolutionary status of the stellar population in the Rho Ophiuchi cloud core, *Astrophys. J.* **438**, 813-829.

Tytler, D. (1995) "Exploration of Neighboring Planetary Systems (ExNPS): Ground Based Element," WWW address: http://techinfo.jpl.nasa.gov/WWW/ExNPS/RoadMap.html. Also in *A Road Map for the Exploration of Neighboring Planetary Systems*,

Jet Propulsion Lab Publication 92-22, Pasadena, CA, 1996.

Ward, W.R. (1996) Survival of planetary systems, *Bull. Amer. Astron. Soc.* **28**, 1112.

Ward, W.R., and K. Hourigan (1989) Orbital migration of protoplanets - The inertial limit, *Astrophys. J.* **347**, 490-495.

Wambsganss, J. (1996) Discovering galactic planets by gravitational microlensing: magnification patterns and light curves, *Mon. Not. Roy. Astron. Soc.* In press.

Weidenschilling, S.J. and F. Marzari (1996) A possible origin of giant planets found at small stellar distances, Submitted to *Nature*.

Wetherill, G. (1994) Possible consequences of the absence of "Jupiters" in planetary systems, In *Planetary Systems: Formation, Evolution and Detection* (B.F. Burke, J.H. Rahe, and E.E. Roettger, Eds.) pp 23-32. Kluwer, Dordrecht.

Witt, H.J. (1990) Investigation of high amplification events in light curves of gravitationally lensed quasars, *Astron. Astrophys* **236**, 311-322.

Zhao, H.S., D.N. Spergel and R.M. Rich (1995) Microlensing by the galactic bar, *Astrophys. J.* **440**, L13-L16.